Myosin-dependent remodeling of adherens junctions protects junctions from Snail-dependent disassembly

Mo Weng[1,2] and Eric Wieschaus[1,2]

[1]Department of Molecular Biology and [2]Howard Hughes Medical Institute, Princeton University, Princeton, NJ 08540

Although Snail is essential for disassembly of adherens junctions during epithelial–mesenchymal transitions (EMTs), loss of adherens junctions in *Drosophila melanogaster* gastrula is delayed until mesoderm is internalized, despite the early expression of Snail in that primordium. By combining live imaging and quantitative image analysis, we track the behavior of E-cadherin–rich junction clusters, demonstrating that in the early stages of gastrulation most subapical clusters in mesoderm not only persist, but move apically and enhance in density and total intensity. All three phenomena depend on myosin II and are temporally correlated with the pulses of actomyosin accumulation that drive initial cell shape changes during gastrulation. When contractile myosin is absent, the normal Snail expression in mesoderm, or ectopic Snail expression in ectoderm, is sufficient to drive early disassembly of junctions. In both cases, junctional disassembly can be blocked by simultaneous induction of myosin contractility. Our findings provide in vivo evidence for mechanosensitivity of cell–cell junctions and imply that myosin-mediated tension can prevent Snail-driven EMT.

Introduction

In both vertebrates and invertebrates, SNAIL transcription factors are the master regulators of epithelial–mesenchymal transitions (EMTs; Lamouille et al., 2014). Expression of SNAIL proteins results in complete disassembly of adherens junctions, a hallmark of EMT, and is an essential step for progression into full mesenchymal state (Huang et al., 2012). In many organisms, junctional disassembly is associated with SNAIL-dependent transcriptional repression of E-cadherin (E-Cad), the major transmembrane component of adherens junctions. During mesodermal EMT in early *Drosophila melanogaster* embryos, junctional disassembly also involves posttranscriptional regulation in which maternally supplied E-Cad protein is eliminated from the junctions. In this system, Snail (Sna) drives junctional disassembly and EMT even when endogenous E-Cad sources have been replaced by E-Cad derived from exogenous promoters (Oda and Tsukita, 2001; Schäfer et al., 2014). The *Drosophila* system therefore provides an opportunity to study the Sna-dependent regulation of adherens junctions at the posttranscriptional level during EMT.

In *Drosophila*, Sna also functions as a primary determinant of mesodermal cell fate and is required for all aspects of early mesoderm behavior (Lim and Thiery, 2012). Intriguingly, although Sna is expressed in mesodermal cells long before gastrulation, neither loss of adherens junctions nor EMT occurs until the tissue completes a stereotyped sequence of shape changes and is internalized (Shishido et al., 1993; Leptin, 1999). This delay in EMT is unlikely to be caused by the time required for Sna to activate target EMT genes, because many known Sna targets are expressed before gastrulation, and the protein product of at least one target gene, Mist, functions during the internalization of mesoderm that precedes the EMT (Shishido et al., 1993; Vincent et al., 1998; Manning et al., 2013; Rembold et al., 2014). Moreover, in certain genetic backgrounds (e.g., *concertina* [*cta*]; *T48* double mutants), a Sna-dependent disassembly of junctions can be observed early during gastrulation (Kölsch et al., 2007), suggesting that Sna targets are expressed in normal development before their effects on junctions are observed. The mechanism that delays Sna's action and the EMT process in wild-type embryos is not known.

The possible reason for the delayed junction loss is that adherens junctions are necessary for the cells to withstand tension in the early stages of gastrulation when cell shape changes in the mesodermal epithelium drive the invagination. These cell shape changes are generated by actomyosin contraction in the apical cortex (Young et al., 1991; Nikolaidou and Barrett, 2004; Dawes-Hoang et al., 2005; Fox and Peifer, 2007; Martin et al., 2009; He et al., 2014) and depend on myosin II contractility (Dawes-Hoang et al., 2005; Xie and Martin, 2015). Myosin contractions occur in pulses that correlate with the reduction of apical area and thus provide a proxy measurement for force generation (Xie and Martin, 2015). The tension force of myosin pulses is transmitted cross the mesodermal tissue through adherens junctions; a compromise of junctional integrity leads to rupture of the tissue and failure of morphogenesis (Sawyer et al., 2009; Martin et al., 2010).

Correspondence to Eric Wieschaus: efw@princeton.edu

Abbreviations used in this paper: E-Cad, E-cadherin; EMT, epithelial–mesenchymal transition.

The Rockefeller University Press $30.00
J. Cell Biol. Vol. 212 No. 2 219–229
www.jcb.org/cgi/doi/10.1083/jcb.201508056

The absence of a thorough description of adherens junction dynamics during *Drosophila* gastrulation contributes to our uncertainties about Sna-dependent junctional disassembly. In tissue culture cells, adherens junctions are thought to exist in a homeostatic relationship with the forces that act on them. Although such cells are generally in steady state, a recent study using suspended cell doublets showed that oscillating myosin II gradients can impose corresponding changes in E-Cad intensity in junctions (Engl et al., 2014). Whether adherens junctions during gastrulation show similar homeostatic changes in response to force is unknown. During normal invagination of *Drosophila*, a switch of junction configurations does in fact occur: adherens junctions change from broadly distributed clusters residing at subapical position to spot-like puncta restricted to the very apical edge of lateral membranes (Dawes-Hoang et al., 2005; Kölsch et al., 2007; Mathew et al., 2011). Although it is assumed that the spot-like apical junctions serve as the connectors for contractile myosin network, it is not known whether those junctions form before or after apical myosin is activated—in other words, whether apical junctions are developed in response to contractile myosin. It is also not known whether formation of apical junctions and disappearance of subapical junctions are independent events or whether apical junctions are made based on subapical junctions. In one model, a Sna-dependent disassembly of subapical junctions is proposed to occur simultaneously with a reassembly of new junctions through an unknown mechanism that is Sna-independent and may involve Traf4 (Kölsch et al., 2007; Mathew et al., 2011).

Here, we used *Drosophila* gastrulating embryos to test the response of adherens junctions to the contractile myosin and its interplay with Sna-driven junction disassembly. We used quantitative live imaging to track individual junctional clusters resolvable by confocal microscopy. The pulsed behavior of myosin contraction allowed us to assess the correlation between junctional properties and actomyosin pulses. The role of myosin on junction properties was tested by genetic approaches.

Results

Adherens junctions are disassembled only after mesodermal invagination despite early expression of Sna

Sna protein can first be detected in the ventral region of the *Drosophila* embryo at the beginning of cycle 14, and its intensity increases as the syncytial embryo undergoes cellularization (Fig. 1, A–D). Consistent with Sna's well-characterized role in promoting junctional disassembly and EMT, E-Cad levels begin to fall in Sna-positive cells during late cellularization (Fig. 1, E and F). In contrast, junctional E-Cad levels in the dorsal region during the same period continue to increase as junctions mature (Fig. 1, G and H). The mesoderm-specific decline in junctional E-Cad levels continues until the onset of gastrulation, when, despite the continued presence of Sna protein, total E-Cad levels begin to increase in association with the cell shape changes that internalize mesoderm. High levels of E-Cad persist in mesodermal junctions until the cells are fully internalized. At that point, myosin II levels decrease, junctions gradually disassemble, and the cells begin a transition to mesenchymal morphology (Fig. 1, I–M). The increase in total E-Cad levels at the beginning of gastrulation could in principle be caused by either increased incorporation of E-Cad in subapical junctions or independent formation of apical junctions and disassembly of subapical junctions. Distinguishing between these models requires following E-Cad accumulations at the level of individual E-Cad clusters.

During junctional remodeling in *Drosophila* gastrulation, individual E-Cad clusters persist and move apically

To determine whether apical junctions in ventral mesodermal cells are built on the subapical junctions or form independently, we need to follow junctional remodeling in detail. During the early phase of ventral furrow formation, both endogenous junctions revealed by Arm (*Drosophila* β-catenin) staining in fixed embryos and junctions labeled by E-Cad::GFP in live embryos show localizations intermediate between subapical and apical positions, suggesting that adherens junctions may move between the two positions as intact clusters (Fig. S1, A and B; and Video 1). We used projection of resliced images and kymographic analyses to visualize the collective behavior of adherens junctions along the apical-basal axis (Fig. 2, A and B; and Video 2). The measured change in the mean position (or intensity-weighted position) of E-Cad::GFP indicates that ∼6 to 7 min are required for junctions to move from subapical to apical position (Fig. 2 C). To definitively demonstrate the direct movement of junctions, individual junctional clusters from edges (junctions on the lateral surfaces shared by two apposing cells) and from vertices (junctions at the point where three cells meet) were tracked manually. We focused on vertex junctions. as they are easier to track and move in one dimension. Four basic behaviors were observed (Fig. 2, D–G; and Video 3). Single clusters can persist and move directly toward the apical edge without dramatically changing morphology (Fig. 2 D). Second, clusters begin with an elongated shape along the apical-basal axis but gradually shrink to a spot (Fig. 2 E). Third, in cases where more than one cluster appears on the same vertex, the basal one catches up with and fuses with the apical cluster (Fig. 2 F). Finally, in some cases, no distinct clusters can be identified at the beginning but clusters are gradually formed during the 5-min movie (Fig. 2 G). During the 5 min when the mean junctional position shifts from subapical to apical, single clusters usually exploit more than one of those four strategies. For example, one cluster could move apically then shrink along the apical-basal axis, or take two actions simultaneously. Among the 55 junction clusters observed in apical positions at the vertices at the end of the 5-min period, 71% were derived from subapical clusters that either were observable at the beginning (47%) or emerged from below the bottom of the stack at some point during the time course (24%). Only 7% of clusters that were initially observed subapically and 20% of the de novo clusters were lost during the 5-min period. The vast majority of clusters therefore persisted from the time when they are observed until the end of the recording. Collectively, these processes shift a broadly distributed subapical junctional domain into a restricted apical spot. A similar process appears to account for the apical accumulation of junctions along cell edges, although because clusters can move laterally and interact with each other they are more difficult to track. However, when clusters on one edge are viewed as a group, the group behaves in the same way as vertex junctions: they move continuously toward the apical side and compact into fewer clusters (Fig. 2 H). Although we cannot distinguish whether the apparent persistence and movement of the junction clusters is caused by the collective movement of all E-Cad molecules in the cluster within the plasma membrane or redistribution

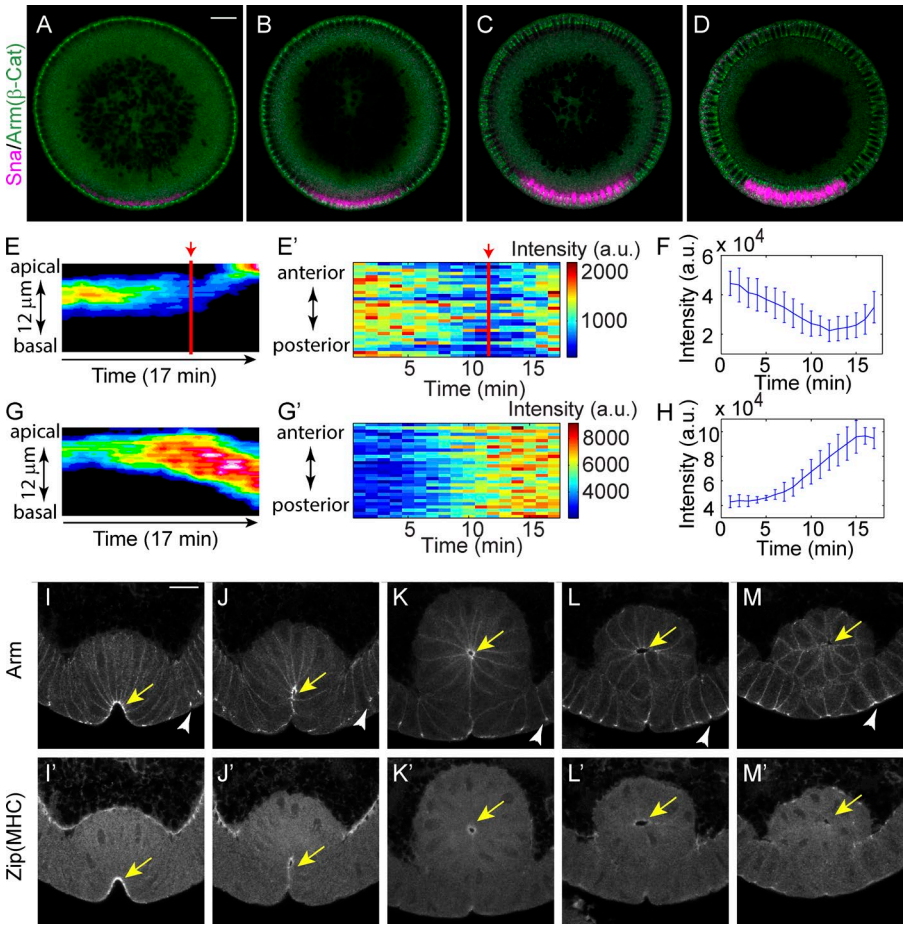

Figure 1. **Early expression of Snail cannot disassemble adherens junctions until the disappearance of apical actomyosin.** (A–D) Expression of Snail protein during early and mid-cellularization. Bar, 20 µm. β-Cat, β-catenin. (E and F) Junction intensity in the ventral cells shows a transient decline until the junctions begin to shift apically. Red lines and arrows indicate the initiation of junction shift. (E) Kymograph of the lateral max projection showing intensity changes. Signals from basal junctions are removed for clarity. (E′) Heat map showing temporal changes in junction intensity. Each stripe at one time point shows the junction intensity along the anterior–posterior axis of a tracked region of interest containing 5(D–V) × 10(A–P) cells around the midline of the mesoderm. (F) Change in total intensity of junctions in the region of interest as in E. Mean and SD from three embryos is shown. (G and H) Changes in junction intensity in dorsal cells during comparable stage. Embryos are aligned in time by the progression of cellularization. (H) Mean and SD from three embryos is shown. a.u., arbitrary units. (I–M) Myosin (myosin II heavy chain [MHC], *zipper* [*zip*]) and junctions (Armadillo/β-catenin) coexist after ventral cell invagination and simultaneously disappear before cells lose their epithelial morphology. Yellow arrows indicate the accumulation of adherens junctions and apical myosin in ventral mesodermal cells. White arrowheads indicate adherens junctions in flanking ectodermal cells. Bar, 15 µm.

of E-Cad via a vesicle-based system, our observation shows that the formation of apical junctions results from the remodeling of subapical junctions rather than being a separate process.

E-Cad density in existing adherens junctions is enhanced as junction clusters shift apically

Junctions that are initially subapical not only persist in the presence of Sna, but also undergo an increase in E-Cad levels as they move apically, in both local density and total intensity (Fig. 3 A). We used the mean and peak intensity within adherens junctions to represent the density of the clusters. Both values increase during this process, implying that E-Cad clusters become more and more densely packed, a change that may enhance their resistance to disruptive force (Fig. 3, B and C; and Fig. S2, A and B). The total intensity of the junctional signal also increases during the same period. This increase is observed even when the effect of clusters emerging from below the scored region is excluded, suggesting that it is caused at least in part by recruitment of more E-Cad molecules into the clusters (Fig. 3, D and E). To test whether new molecules are also added to replace the old ones, we performed FRAP experiments. When junctions are bleached shortly before the junctional change, the intensity recovers to a level very close to that of unbleached neighboring regions in ∼12 min (Fig. 3 F). Because the total intensity of junctions increases during this process, junctions are not in a steady state, and thus we could not obtain the exact turnover rate of E-Cad molecules. However, we can use the difference in fluorescence between the bleached region and the control region to determine the amount of E-Cad molecules that are bleached but have not yet been replaced by new E-Cad molecules. We specifically examined E-Cad recovery during the time window of junction shift as determined by mean junction position measurement in the control region. About half of the E-Cad intensity bleached at the beginning of the junction shift is recovered within 5 min, a rate faster than that measured in dorsal cells of comparably staged embryos (Fig. 3 G). The remaining bleached E-Cad molecules are retained in the junctions. This retention might occur either if bleached E-Cad molecules move directly with the junction cluster to the apical position or if they are recycled back to the junction cluster during a disassembly and reassembly process. Thus, although the whole cluster persists and moves, E-Cad molecules inside the cluster are rapidly being taken off and replenished, a dynamic that may allow for restructuring the junctions and increasing their density.

Junctional remodeling is temporally correlated with myosin activity

If the junctional changes described are triggered by myosin activation, they should be temporally correlated with myosin activation during ventral furrow formation, with respect to both developmental timing and individual myosin pulses (Martin et al., 2009). Because myosin activity is essential for its localization to the apical cortex at gastrulation stage (Young et al., 1991; Nikolaidou and Barrett, 2004; Dawes-Hoang et al., 2005; Fox and Peifer, 2007; Martin et al., 2009; He et al., 2014), its accumulation indicates some level of activation, and its intensity has been shown to correlate with apical constriction and thus with the tension force that drives ventral furrow formation (Xie and Martin, 2015). We therefore used the mCherry-tagged

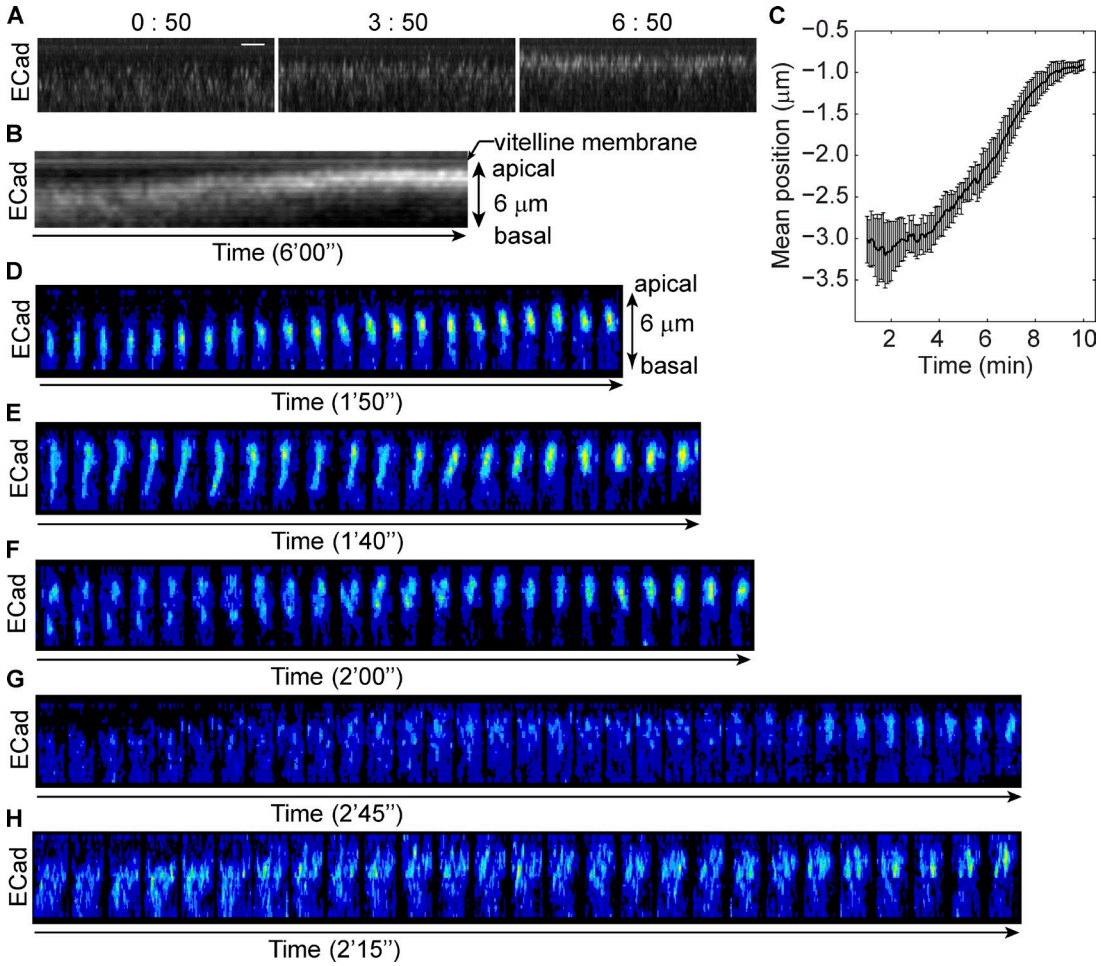

Figure 2. **Adherens junctions move directly from subapical position to apical position.** (See also Fig. S1 and Videos 1–3.) (A) Projections of resliced stacks show the position and intensity change of E-Cad::GFP in a living embryo. Bar, 2 µm. (B) Kymograph of E-Cad::GFP shows continued movement of junctions. (C) The change of mean position of junctions during apical constriction as indicated by the distance below the vitelline membrane (position of vitelline membrane is defined as 0 µm). $n = 5$. (D–H) Junction clusters on single vertex or edge visualized by E-Cad::GFP. Each tile is a 3D reconstructed image, and tiles are 5 s apart in time. Only the time periods exclusively showing a single mode of movement are shown. (D) A single junction cluster moves from subapical to apical position. (E) A junction cluster shrinks along the apical-basal axis. (F) Two junction clusters on a single vertex move apically while the more basal one catches up and fuses with the more apical one. (G) Junction clusters form de novo around apical position. (H) Clusters on a single edge move apically as a group.

myosin II regulatory light chain (*spaghetti squash* [*sqh*]) to indicate the activity of myosin II in live embryos. Dual-color live imaging of junctions and myosin shows that adherens junctions remain at subapical positions until myosin begins to accumulate and mesodermal cells begin to converge toward the midline of the future furrow (Fig. 4, A and B). The convergence toward the midline reflects the reduction in apical area associated with actomyosin-generated force (Martin et al., 2010; Xie and Martin, 2015). Thus adherens junctions are repositioned and remodeled while they are under myosin-generated tension. This also indicates that actomyosin fibers can engage subapical junctions, most likely through the continuity of the lateral actin cortex with the apical medial region of the cell allowed by their dome-shaped apical surface at the beginning of gastrulation (Sweeton et al., 1991; Dawes-Hoang et al., 2005).

By examining the junctions in individual vertices and edges, we found that junction features change in pulses with a periodicity similar to that previously described for myosin contractile behavior (Martin et al., 2009; Fig. 4, C and D). Changes in the mean position, total intensity, and density of adherens junctions on individual edges and vertices correlate temporally with pulses of myosin intensity in their vicinity (Fig. 4, E–J). A previous study focused on the myosin on the medial region of the apical cortex as providing the mechanical tension to drive mesoderm cell shape change (Martin et al., 2009). By the gastrula stage in our preparations, we observed that myosin also accumulates at the junctions themselves as medial myosin accumulates in their vicinity (Fig. 4, M and N). Both the medial myosin in proximity and the myosin accumulated at the junctions themselves correlate with the changes in the junctional features we have examined. These two pools of myosin temporally correlate with each other as well, with pulses of nonjunctional medial myosin slightly preceding junctional myosin (Fig. 4, K and L). Consistent with the time lag between the two pools of myosin, fluctuations of nonjunctional myosin consistently precede changes in junction features, whereas the changes in junctional myosin only slightly precede or coincide with junctional changes (Fig. 4, E–J). This suggests that the medial myosin that reaches the junctions may be the source that triggers the myosin accumulations in the junctions themselves.

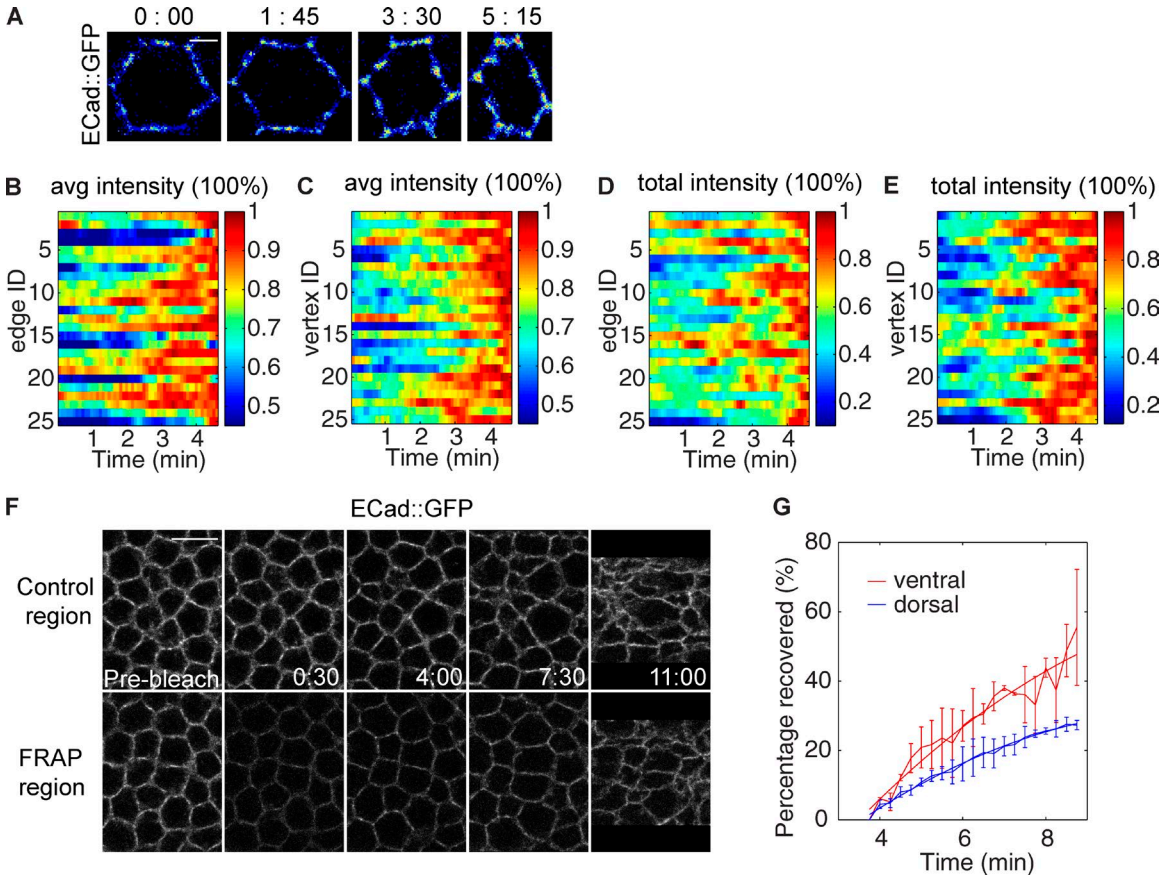

Figure 3. **Adherens junctions are enhanced in total intensity and density during the apical shift.** (See also Fig. S2.) (A) Projections of a single cell visualized by E-Cad::GFP show the change in intensity and density of the junctions during gastrulation. Bar, 2 µm. (B and C) Changes in the mean intensity of E-Cad signal at individual edge (B) and vertex (C) junctions (averaged by the number of nonzero pixels after image thresholding). (D and E) Changes in the total amount of E-Cad at individual edge (D) and vertex (E) junctions. For B–E, the values at different time points of each edge or vertex sample are normalized by the maximum value of that edge or vertex during the time period presented. (F) A FRAP region compared with an unbleached control region in the same embryo. Bar, 10 µm. (G) The percentage of bleached molecules recovered from the beginning of junction shift, calculated by comparing fluorescence intensity in the control and bleached regions. FRAP was performed on three embryos for both dorsal and ventral regions.

The impact of myosin on junctional morphology is local in nature: no obvious correlation is found when junction measurements from one edge or vertex are paired with myosin measurements from a different edge or vertex (Fig. S3 A). Furthermore, as another negative control, we tested for correlation between junctional properties and the low sporadic myosin activity occasionally observed in dorsal cells in wild-type embryos (Wang et al., 2012). Although there is fluctuation in junctional properties and occasional flashes of myosin in wild-type dorsal cells, no correlation can be observed between myosin activity and junctional changes (Fig. S3 B).

Junction remodeling requires myosin, and ectopic activation of myosin recapitulates the junction behavior of ventral cells

Next we tested whether myosin II is responsible for the persistence and enhancement of adherens junctions in mesoderm despite the presence of Sna. When myosin levels are strongly reduced by RNAi, almost all junction signal is lost in mesodermal cells, suggesting that contractile myosin is required for junction maintenance in this tissue (Fig. 5, A and B). This phenotype is similar to that previously observed in *cta*; *T48* mutants, in which myosin expression is normal but the protein fails to accumulate apically (Kölsch et al., 2007). To examine the role of myosin in junction repositioning, we used RNAi lines causing moderate reductions in myosin levels, such that junctions are not completely abolished and ventral cells still invaginate, but at a reduced rate. Under these conditions, it takes almost twice as long for adherens junctions to move from their subapical position to an apical position, and the junction intensity is reduced (Fig. 5, C and D).

We tested whether ectopic activation of myosin contraction in other cell types is sufficient to induce the same behavior of junction clusters. To induce ectopic myosin contraction, we used expression of *folded gastrulation* (*fog*), the factor secreted by the ventral cells to activate actomyosin contraction (Costa et al., 1994; Morize et al., 1998; Dawes-Hoang et al., 2005). We chose to examine the dynamics of E-Cad clusters in dorsal cells with heat shock–controlled Fog overexpression because wild-type dorsal cells during early gastrulation do not show significant myosin (Wang et al., 2012). Upon activation of myosin contraction, E-Cad clusters persist and move continuously to the apical edge of the lateral membrane, reminiscent of the junction behavior in ventral cells described previously (Fig. 5 E). As ectodermal cells do not express Sna, this result indicates that the disappearance of subapical junctions does not require Sna-dependent disassembly. Meanwhile, the total intensity and the density of junctions also change in a correlation with myosin

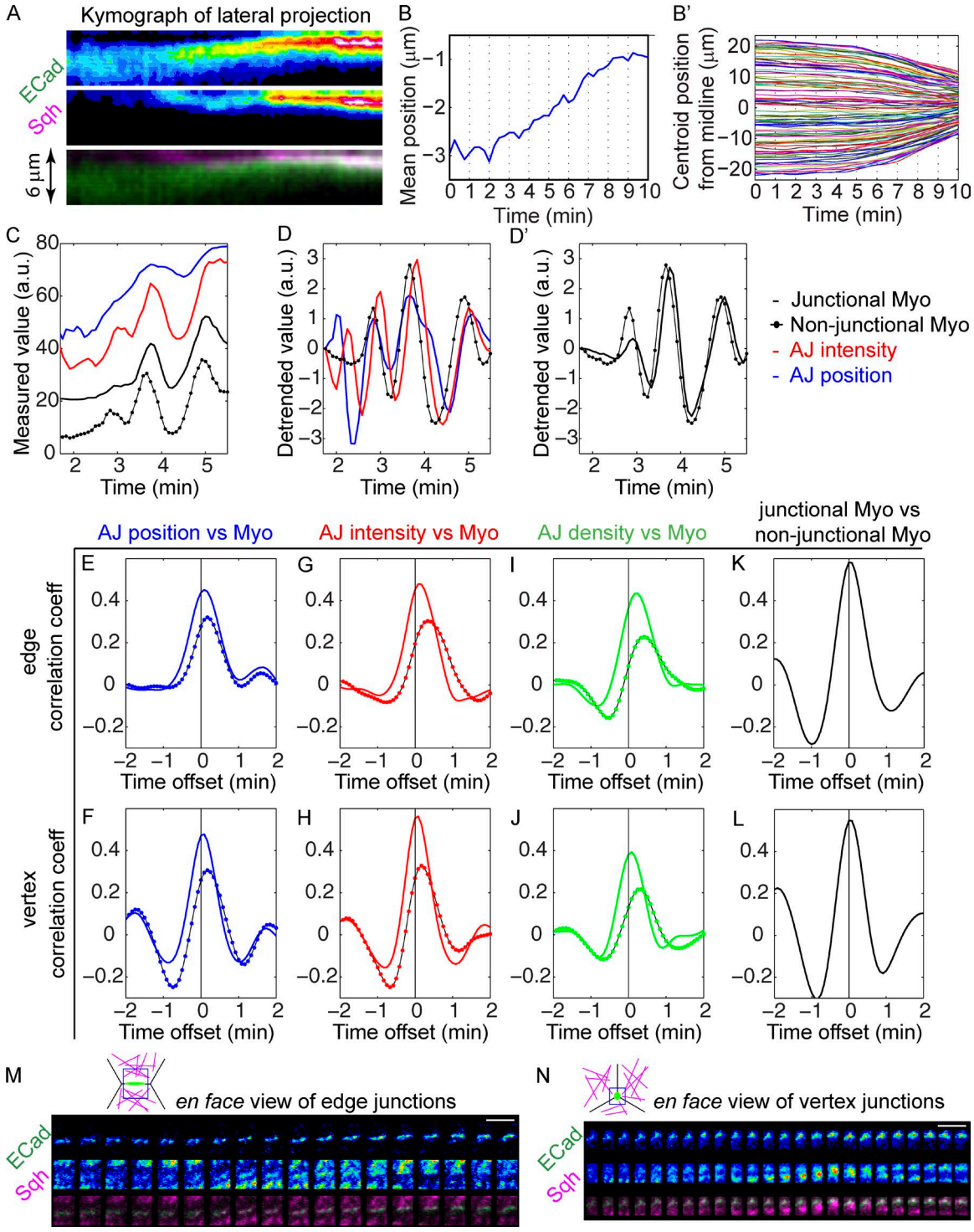

Figure 4. **Features of adherens junctions change in pulses and are temporally correlated with myosin activity in ventral cells.** (See also Fig. S3.) (A) Kymographs of E-Cad::GFP and Sqh::mCherry from lateral projections shows junctions begin to move apically and become more intensified upon the apical accumulation of apical myosin. (B) Initiation of junction shift (junction mean position) coincides with cell convergence toward the D–V midline of mesodermal epithelium in the same embryo (B′). 102 mesoderm cells from the same embryo were analyzed. (C and D) An example of the measurements of mean position and total intensity of the tracked junctions and the intensity of junctional myosin and nonjunctional myosin. (D and D′) Data in C are detrended to reveal the pulses of each measurement (see Materials and methods). (D) The overlapping peaks of junction parameters and myosin. Only nonjunctional myosin is shown for clarity. (D′) Junctional myosin and nonjunctional myosin show similar changes. Temporal resolution: 5 s. a.u., arbitrary units. (E–J) Mean correlation coefficients between junction features and myosin intensity in ventral cells (n = 30). Colored solid lines: correlation with the junctional myosin. Solid lines with colored dots: correlation with nonjunctional myosin. Mean intensity of E-Cad signal is used as the junction density. (K and L) Temporal correlations between junctional myosin and nonjunctional myosin. (E, G, I, and K) Analysis of edge junctions. (F, H, J, and L) Analysis of vertex junctions. AJ, adherens junction; Myo, myosin. (M and N) En face views of the tracked junctions and their surrounding medial myosin showing junctional myosin accumulates as medial myosin approaches the junctions. (M) Edge junctions. (N) Vertex junctions. Cartoons show the position of the region of interest relative to the cells: junctions in green, myosin in magenta, and region of interest in blue. Bars, 5 µm. n = 30.

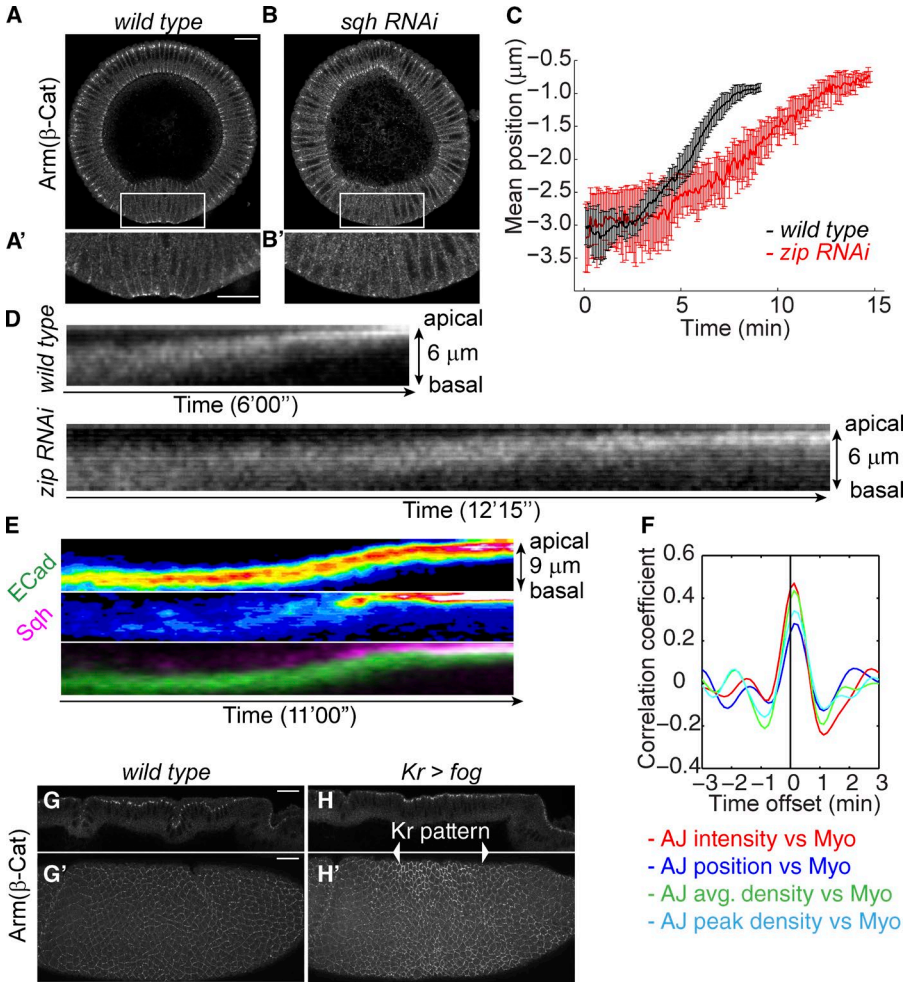

Figure 5. **Myosin is required for the junctional remodeling and ectopic activation of myosin remodels junctions in a manner recapitulating that of mesodermal cells.** (See also Fig. S4.) (A and B) Strong myosin RNAi (*sqh* RNAi) leads to loss of adherens junctions. Bar, 20 µm. (A′ and B′) Zoom-in images of the ventral cells. Bar, 20 µm. (C) Comparison between wild-type and moderate myosin RNAi (RNAi against *zip*) embryos on the time required for the junction shift. $n = 5$ for wild-type and $n = 4$ for *zip* RNAi. (D) Kymographs of E-Cad::GFP in ventral cells of wild-type and *zip* RNAi embryos. (E) Kymographs of E-Cad::GFP and Sqh::mCherry in dorsal cells with ectopic myosin contraction. (F) Mean correlation coefficients between myosin activity and junctional features in dorsal cells expressing Fog. The intensity of myosin including junctional and nonjunctional myosin is used here for correlation analysis. $n = 26$. (G and H) Arm staining in a wild-type (G) and a kr>fog (H) embryo. G and H are midsagittal sections of dorsal cells. G′ and H′ are max projections of the lateral surface of the embryos. Bars, 20 µm. β-Cat, β-catenin; AJ, adherens junctions; Myo, myosin.

pulses (Fig. 5 F). Myosin is responsible for the phenotype, as knockdown of myosin suppresses the junction shift induced by Fog overexpression (Fig. S4). To further confirm that activation of apical myosin can locally increase junction intensity and density, we generated a stripe of apical myosin by expressing Fog using kr-gal4. Within the Fog-expressing zone, junctions showed a higher intensity than those outside the zone (Fig. 5, G and H). These results suggest that myosin contraction not only induces intensity reinforcement of adherens junctions in ventral mesodermal cells, but also can do so in epithelial tissues not programmed to mesodermal fate and expressing no Sna.

Contractile myosin protects junctions from Sna-driven junction disassembly

In the myosin knockdown experiments described, the loss of junctions is observed only in ventral cells, although myosin levels are reduced over the entire embryo. In contrast, junctions in ectodermal cells of the same embryo remained strong (Fig. 6 A). Because Sna is normally expressed in mesodermal but not ectodermal cells, the loss of junctions in mesoderm is consistent with a Sna-dependent EMT. To test this possibility, we overexpressed Sna in ectodermal cells and found that high levels of Sna are sufficient to weaken or eliminate junctions in ectodermal cells (Fig. 6, B and C). In these experiments, induced Sna accumulation had minimal effect on junctions in mesodermal cells, where Sna was already expressed but coincident with myosin contractility. These observations raise the possibility that actomyosin contraction may antagonize Sna-dependent junction disassembly. We tested this by simultaneous expression of Fog and Sna in the ectoderm. We found that Fog overexpression is able to restore junctions in Sna-expressing ectodermal cells (Fig. 6 D). Our results suggest that in the mesoderm, junctions would not be disassembled until the disappearance of contractile myosin. This is consistent with our observation that junction disassembly and apical myosin loss occur simultaneously and only after invagination is completed (Fig. 1, L and M). Collectively, these results suggest that contractile myosin on junctions might reorganize junctional structure in a way that maintains junctional integrity even in the presence of Sna.

Discussion

Here we show that during *Drosophila* gastrulation, subapical junctions are repositioned toward the apical surface and are strengthened as the cortical tension increases. Both these phenomena follow apical myosin activation and thus may reflect a mechanosensitive response of junctional complexes to the tension generated by this activation of myosin. The junctional responses occur on the time scale of individual myosin pulses and are temporally correlated with those pulses. Such junctional changes depend on myosin activity but do not require Sna, given that ectopic myosin activation recapitulates similar junctional responses in Sna-negative tissues. This phenomenon may not

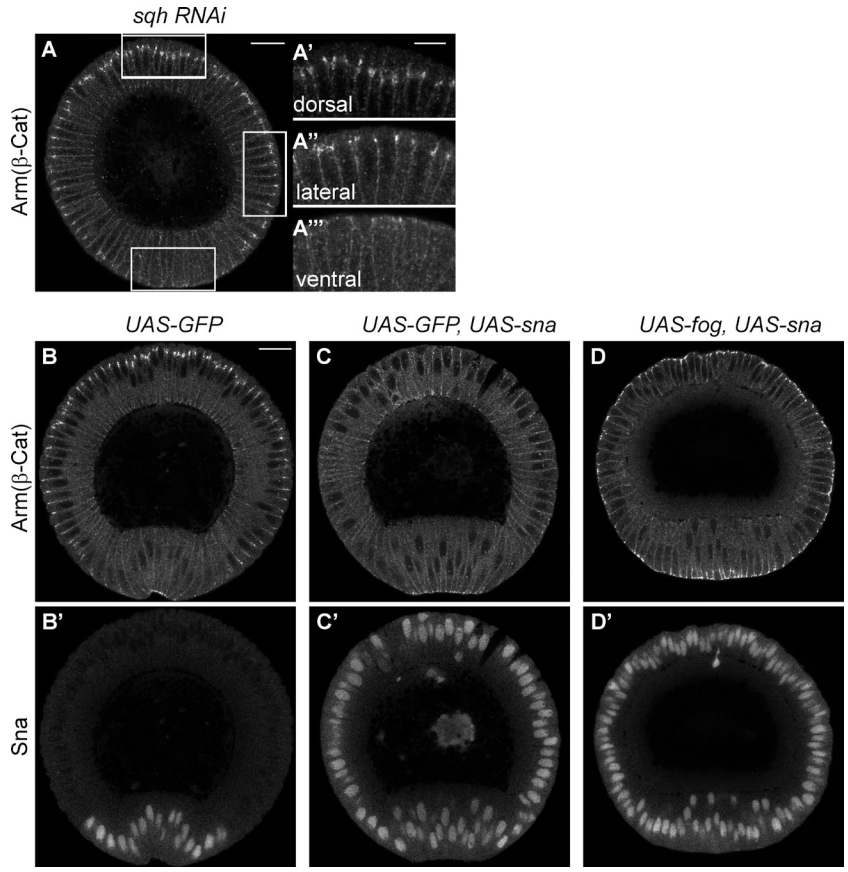

Figure 6. **Myosin contractility suppresses Sna-dependent junction disassembly.** (A) Strong myosin RNAi (*sqh* RNAi) leads to junction loss only in mesodermal cells (ventral) but not in ectodermal cells (dorsal and lateral). Bar, 20 µm. (A′–A‴) Enlarged images of ventral, lateral and dorsal cells, respectively. Bar, 10 µm. (B) Junctions stained by Arm in control embryos with GFP expression. (C) Misexpression of Sna in the whole embryo causes junction loss in ectodermal cells, whereas junctions in apically constricting ventral cells remain. (D) Myosin activation in the whole embryo restores junctions in the presence of Sna misexpression. (C′ and D′) Sna staining in the same embryos as C and D. Bar, 20 µm. β-Cat, β-catenin.

be restricted to *Drosophila* embryos. The increased contractile actomyosin on the apical cortex of human cell lines deficient for the cortex actin regulator Merlin is associated with a condensation of adherens junctions toward the apical surface, suggesting that the response of adherens junctions to cortical tension can be of general significance (Chiasson-MacKenzie et al., 2015).

The changes in junction mass and density suggest that, rather than being simple passive anchors for contractile actomyosin filaments, adherens junctions respond to the contractile actomyosin by restructuring and repositioning themselves, potentially involving aggregation and rearrangement of E-Cad molecules within the plasma membrane or vesicle-based redistribution of E-Cad. Indeed, actomyosin organization has been shown to be critical in the lateral clustering of E-Cad molecules (Cavey et al., 2008; Truong Quang et al., 2013; Wu et al., 2014; Chen et al., 2015). The change in E-Cad clustering is considered an active mechanosensitive mechanism to strengthen the adhesion (Smutny et al., 2010; Engl et al., 2014; Lecuit and Yap, 2015). Alternatively, the adhesion can also be remodeled through the vesicle-based mechanisms, and endocytosis of E-Cad has been shown to be up-regulated when junctions are under actomyosin-generated stress (Levayer et al., 2011). The repositioning could also arise through restructuring rather than passive dragging, if for example recycling and turnover rates in the basal regions of the junctions differ from apical regions. Overall, regardless of the underlying mechanism, this mechanosensitivity may be advantageous, providing a direct self-corrective mechanism that allows junctions to adjust their localization and intensity to match the mechanical force they experience.

Although the molecular mechanism for the junction strengthening requires further investigation, our data suggest that it is resistant to the posttranscriptional disassembly of adherens junctions downstream of Sna. The phenotype of myosin knockdown in this study resembles that previously described for *cta*; *T48* double mutants, in which apical actomyosin cannot be activated and junctions are lost only in the ventral mesodermal cells (Kölsch et al., 2007). In all scenarios in which Sna expression is associated with junction loss (ventral cells in *cta; T48* mutants, ventral cells in myosin knockdown mutants, and ectodermal cells with ectopic Sna expression), Sna is expressed in cells in the absence of myosin contractility. Maintenance of adherens junctions ultimately relies on the balance between assembly and disassembly rates of junctional components. Thus mechanical force likely modulates the assembly/disassembly balance and therefore remains in a homeostatic relationship with the junctions bearing the force.

In the early stages of embryogenesis analyzed in this study, E-Cad is maternally provided and thus not subject to direct transcriptional repression. The disassembly of junctions in the absence of myosin contraction must therefore reflect a posttranscriptional regulation on junctions, likely performed by one or several of Sna's transcriptional targets. Much effort has been invested in identifying transcription targets of Sna, but it is not known which, if any, of its known targets might play such a role. One mesodermally expressed gene, *Traf4*, is required for fine-tuning junction morphology, but its expression appears to depend on the other mesodermal determinant, Twist, rather than Sna (Mathew et al., 2011). One gene repressed by Sna in *Drosophila* mesoderm, *bearded*, is required for the subapical positioning of adherens junctions in cells not expressing Snail (Chanet and Schweisguth, 2012). It is not clear, however, whether Bearded plays a direct role in junction disassembly or

a more general role in apical polarity or the apical myosin contractility that drives repositioning. The posttranscriptional regulation of adherens junction disassembly may allow more rapid and effective EMT than a disassembly relying on transcriptional down-regulation of junctional components such as E-Cad. Identifying and characterizing the relevant Sna targets in *Drosophila* may provide insights into the underlying mechanism for this disassembly, especially with respect to its apparent sensitivity to externally exerted tension. The force-dependent resistance to this Sna function may help in dissecting the underlying molecular functions. Further exploration of Sna's posttranscriptional effect on junctions and how myosin contraction antagonizes Sna will shed light on our understanding of EMT processes.

Materials and methods

Fly stocks and genetics

Maternal driver line *mat^{67};mat^{15}* carries matα4-GAL-VP16 (Häcker and Perrimon, 1998) in homozygous inserts on II and III. When genes are maternally expressed, virgin females of *UAS* lines are crossed to males of *mat^{67};mat^{15}*, and F1 females are crossed to males of appropriate genotypes to produce embryos with maternally loaded gene products. The following stocks expressing fluorescent proteins were used either independently or after being recombined with maternal driver line: *ubi-dE-Cad::GFP* (Oda and Tsukita, 2001) and *sqh::mCherry* (Martin et al., 2009). *y, w, sqh^{AX3}; shg, ubi-dE-Cad::GFP; sqh::mCherry* was made for dual-color live imaging. Fog was expressed zygotically by crossing appropriate females to males of *hs-fog^{5}* (Morize et al., 1998) or *UAS-fog^{9A}* (Dawes-Hoang et al., 2005). RNAi lines—*sqh* RNAi (stock #32439) and *zip* RNAi (stock #37480)—were obtained from the Transgenic RNAi Project at Harvard Medical School and maternally expressed using *mat^{67};mat^{15}* or *w; mat^{67};mat^{15}, ubi-E-Cad::GFP* for live imaging. *UAS-sna* and *UAS-GFP* were expressed maternally using *mat^{67};mat^{15}*. *wy; kr-Gal4/TM3, Sb* was obtained from B. Shilo's laboratory, originally made by M. Leptin's laboratory (Castelli-Gair et al., 1994).

Live imaging

Embryos were dechorionated in 50% bleach, washed in water, and mounted in glass-bottom Petri dishes by the natural affinity between vitelline membrane and glass. The dish chamber was then filled with water and covered by an oxygen-permeable membrane. Images were acquired on a Leica SP5 confocal microscope with a 63×/1.4 NA oil lens. An argon ion laser and a 561-nm diode laser were used to excite GFP and mCherry, respectively. Images for junction cluster tracking was acquired at 4× magnification and a resolution of 120 nm per pixel in *z*-stacks starting from the ventral surface of the embryo to 6 µm deep with 0.5-µm increments, at a temporal resolution of 5 s per *z*-stack, with pinhole set at 1 Airy unit. For FRAP experiments, the region of interest was bleached from the embryo surface to 8 µm deep at one time point, and *z*-stacks of 15 µm were taken at a spatial resolution of 150 µm per pixel and a temporal resolution of 15 s.

Embryo fixation and fluorescent microscopy

Embryos were dechorionated with 50% bleach and fixed by heat-methanol protocol as described (Müller and Wieschaus, 1996). In brief, embryos were incubated in a boiling salt solution containing 0.03% Triton X-100 and 0.4% NaCl for 10 s and quickly cooled by addition of ice and chilled salt solution. Vitelline membranes were removed by shaking the embryos vigorously in 1:1 heptane/methanol. Primary antibodies used were mouse anti-Arm (N2-7A1, DSHB, 1:50), rat and guinea pig anti-Sna (1:1,000, Wieschaus's laboratory), and rabbit anti-Zip (1:100, Wieschaus's laboratory). Secondary antibodies conjugated with Alexa Fluor 488, 568, and 647 were used (Molecular Probe). Stained embryos were sorted and cross-sectioned by hand (using a 26-gauge hypodermic needle) in 50% Aquapolymount/PBS-Tween and mounted in Aquapolymount (Polysciences). Images were acquired on an SP5 confocal microscope (Leica) with a 20× or 63×/1.3 NA glycerol immersion lens.

Imaging processing and analysis

All images for publication were processed in ImageJ. Brightness and contrast may be adjusted across the whole image for better visualization. Quantitative analysis was done using MATLAB (MathWorks). Images were processed to subtract the background before quantitative analysis. To determine the background value for myosin, cytoplasmic myosin intensity below the apical cortex was measured, and the mean was calculated over multiple cells at each time point. The mean plus two SDs of the measurement was used for background subtraction of the images from myosin channel. Background of E-Cad signal was determined by measuring the intensity of freely diffusible E-Cad on the lateral membranes below the junctional region, and the mean plus two SDs was used as the background value. Image segmentation was performed by the custom MATLAB program EDGE, which automatically detects and converts cell membranes into cell edges. Cell centroid position was also obtained through EDGE (Gelbart et al., 2012; see data files in the online supplemental material).

To quantify junction total intensity in embryos developing from cellularization to early gastrulation, a 15-µm-thick *z*-stack was imaged with a temporal resolution of 1 min. When the images were processed for quantifying the junction intensity, a region of interest was drawn at each time point to always include the same cells (~5 × 10 cells). To obtain the heat map, the stack at each time point was first projected by summing the pixel intensities along the *z* axis. The D–V axis of the 2D dataset was collapsed by summing the intensities along the D–V axis, resulting in a 1D dataset of intensities along the A–P axis at each time point. Sums for every five pixels along the A–P axis were obtained and are presented as one vertical stripe at each time point in the heat map. The total intensity curve was obtained by summing all the pixel intensities at each time point and taking the mean values over three embryos. Embryos imaged for ventral and dorsal regions were aligned by the initiation of cellularization. The initiation of gastrulation is defined as the time when ventral cells start to converge to the midline of the ventral furrow.

Mean position is calculated as intensity-weighted positions (i.e., the sum of $Int_i * z_i$, where Int_i and z_i denote fluorescence intensity and depth of the stack section, respectively), normalized by total fluorescence intensity (sum of Int_i).

Junction clusters on individual vertex or edge were identified manually from the apical-basal stacks described in the Live imaging section. A region of interest exclusively containing the junctions was drawn manually, and the coordinates were recorded using a custom ImageJ macro. Individual *z*-stacks were extracted from both E-Cad and myosin channels based on coordinates using MATLAB, and junction features and myosin intensity were quantified within this stack of interest. Images were first thresholded as described previously. For junction density measurement, only the nonzero pixels were used. Junctional myosin was segmented using the mask generated from the junction signal. Nonjunctional myosin intensity was quantified by subtracting the junctional myosin intensity from the total myosin intensity in the stack of interest. Images of the junctions were 3D reconstructed at each time point from the same stacks using a custom ImageJ macro for visualization. All original data were first smoothed using a moving mean filter with span set at seven and 30 time points, respectively. The

detrended data were obtained by normalizing the 7–time point smoothed data with the 30–time point smoothed data at individual time points. The resulting dataset was shifted along the *y* axis by 1 to suit for cross-correlation analysis using MATLAB built-in functions.

Online supplemental material

Fig. S1 shows the intermediate positions of adherens junctions during junction remodeling in both fixed and live embryos. Fig. S2 shows the measurements of the peak intensity of adherens junctions on individual edges and vertices. Fig. S3 shows the negative controls of the temporal correlation analysis between myosin intensity and junctional features. Fig. S4 shows that myosin is responsible for the junction phenotypes induced by Fog overexpression. Video 1 shows the en face view of adherens junctions in ventral cells at different depths during junction shifts. Video 2 shows the apical-basal movement of adherens junctions in ventral cells from a lateral view. Video 3 shows movement of individual junction clusters. EDGE program was developed by Gelbart et al. (2012) and is publicly available at the https://code.google.com/p/embryo-development-geometry-explorer/. ImageJ plugin ROI_coordinates functions to output the *x*, *y* coordinates of the manually drawn regions of interest to a .txt file. ImageJ plugin 3D_Tile functions to generate 3D projections of the stacks using the coordinates of the regions of interest and tile the projections by their temporal sequences. Online supplemental material is available at http://www.jcb.org/cgi/content/full/jcb.201508056/DC1.

Acknowledgments

We thank the Bloomington *Drosophila* Stock Center for fly stocks. We thank members of the Wieschaus and Schupbach laboratories, especially for discussion and helpful comments. We acknowledge K. Dourovinski for help on ImageJ macros. We thank Z. Zhu for help on correlation analysis. We thank Y.-C. Wang, B. He, M. Osterfield, and M. Swan for helpful comments on the manuscript. We are indebted to the staff of the Imaging Facilities of the Princeton Molecular Biology department and Lewis Sigler Institute.

This work was supported in part by grant 5R37HD15587 from National Institute of Child Health and Human Development to E.F. Wieschaus and New Jersey Commission on Cancer Research Postdoctoral Fellowship to M. Weng. E.F. Wieschaus is an investigator with the Howard Hughes Medical Institute.

The authors declare no conflicts of interest.

Submitted: 14 August 2015
Accepted: 10 December 2015

References

Castelli-Gair, J., S. Greig, G. Micklem, and M. Akam. 1994. Dissecting the temporal requirements for homeotic gene function. *Development.* 120:1983–1995.

Cavey, M., M. Rauzi, P.F. Lenne, and T. Lecuit. 2008. A two-tiered mechanism for stabilization and immobilization of E-cadherin. *Nature.* 453:751–756. http://dx.doi.org/10.1038/nature06953

Chanet, S., and F. Schweisguth. 2012. Regulation of epithelial polarity by the E3 ubiquitin ligase Neuralized and the Bearded inhibitors in *Drosophila*. *Nat. Cell Biol.* 14:467–476. http://dx.doi.org/10.1038/ncb2481

Chen, C.S., S. Hong, I. Indra, A.P. Sergeeva, R.B. Troyanovsky, L. Shapiro, B. Honig, and S.M. Troyanovsky. 2015. α-Catenin-mediated cadherin clustering couples cadherin and actin dynamics. *J. Cell Biol.* 210:647–661. http://dx.doi.org/10.1083/jcb.201412064

Chiasson-MacKenzie, C., Z.S. Morris, Q. Baca, B. Morris, J.K. Coker, R. Mirchev, A.E. Jensen, T. Carey, S.L. Stott, D.E. Golan, and A.I. McClatchey. 2015. NF2/Merlin mediates contact-dependent inhibition of EGFR mobility and internalization via cortical actomyosin. *J. Cell Biol.* 211:391–405. http://dx.doi.org/10.1083/jcb.201503081

Costa, M., E.T. Wilson, and E. Wieschaus. 1994. A putative cell signal encoded by the folded gastrulation gene coordinates cell shape changes during *Drosophila* gastrulation. *Cell.* 76:1075–1089. http://dx.doi.org/10.1016/0092-8674(94)90384-0

Dawes-Hoang, R.E., K.M. Parmar, A.E. Christiansen, C.B. Phelps, A.H. Brand, and E.F. Wieschaus. 2005. Folded gastrulation, cell shape change and the control of myosin localization. *Development.* 132:4165–4178. http://dx.doi.org/10.1242/dev.01938

Engl, W., B. Arasi, L.L. Yap, J.P. Thiery, and V. Viasnoff. 2014. Actin dynamics modulate mechanosensitive immobilization of E-cadherin at adherens junctions. *Nat. Cell Biol.* 16:587–594. http://dx.doi.org/10.1038/ncb2973

Fox, D.T., and M. Peifer. 2007. Abelson kinase (Abl) and RhoGEF2 regulate actin organization during cell constriction in *Drosophila*. *Development.* 134:567–578. http://dx.doi.org/10.1242/dev.02748

Gelbart, M.A., B. He, A.C. Martin, S.Y. Thiberge, E.F. Wieschaus, and M. Kaschube. 2012. Volume conservation principle involved in cell lengthening and nucleus movement during tissue morphogenesis. *Proc. Natl. Acad. Sci. USA.* 109:19298–19303. http://dx.doi.org/10.1073/pnas.1205258109

Häcker, U., and N. Perrimon. 1998. DRhoGEF2 encodes a member of the Dbl family of oncogenes and controls cell shape changes during gastrulation in *Drosophila*. *Genes Dev.* 12:274–284. http://dx.doi.org/10.1101/gad.12.2.274

He, B., K. Doubrovinski, O. Polyakov, and E. Wieschaus. 2014. Apical constriction drives tissue-scale hydrodynamic flow to mediate cell elongation. *Nature.* 508:392–396. http://dx.doi.org/10.1038/nature13070

Huang, R.Y., P. Guilford, and J.P. Thiery. 2012. Early events in cell adhesion and polarity during epithelial-mesenchymal transition. *J. Cell Sci.* 125:4417–4422. http://dx.doi.org/10.1242/jcs.099697

Kölsch, V., T. Seher, G.J. Fernandez-Ballester, L. Serrano, and M. Leptin. 2007. Control of *Drosophila* gastrulation by apical localization of adherens junctions and RhoGEF2. *Science.* 315:384–386. http://dx.doi.org/10.1126/science.1134833

Lamouille, S., J. Xu, and R. Derynck. 2014. Molecular mechanisms of epithelial-mesenchymal transition. *Nat. Rev. Mol. Cell Biol.* 15:178–196. http://dx.doi.org/10.1038/nrm3758

Lecuit, T., and A.S. Yap. 2015. E-cadherin junctions as active mechanical integrators in tissue dynamics. *Nat. Cell Biol.* 17:533–539. http://dx.doi.org/10.1038/ncb3136

Leptin, M. 1999. Gastrulation in *Drosophila*: The logic and the cellular mechanisms. *EMBO J.* 18:3187–3192. http://dx.doi.org/10.1093/emboj/18.12.3187

Levayer, R., A. Pelissier-Monier, and T. Lecuit. 2011. Spatial regulation of Dia and Myosin-II by RhoGEF2 controls initiation of E-cadherin endocytosis during epithelial morphogenesis. *Nat. Cell Biol.* 13:529–540. http://dx.doi.org/10.1038/ncb2224

Lim, J., and J.P. Thiery. 2012. Epithelial-mesenchymal transitions: Insights from development. *Development.* 139:3471–3486. http://dx.doi.org/10.1242/dev.071209

Manning, A.J., K.A. Peters, M. Peifer, and S.L. Rogers. 2013. Regulation of epithelial morphogenesis by the G protein-coupled receptor mist and its ligand fog. *Sci. Signal.* 6:ra98. http://dx.doi.org/10.1126/scisignal.2004427

Martin, A.C., M. Kaschube, and E.F. Wieschaus. 2009. Pulsed contractions of an actin-myosin network drive apical constriction. *Nature.* 457:495–499. http://dx.doi.org/10.1038/nature07522

Martin, A.C., M. Gelbart, R. Fernandez-Gonzalez, M. Kaschube, and E.F. Wieschaus. 2010. Integration of contractile forces during tissue invagination. *J. Cell Biol.* 188:735–749. http://dx.doi.org/10.1083/jcb.200910099

Mathew, S.J., M. Rembold, and M. Leptin. 2011. Role for Traf4 in polarizing adherens junctions as a prerequisite for efficient cell shape changes. *Mol. Cell. Biol.* 31:4978–4993. http://dx.doi.org/10.1128/MCB.05542-11

Morize, P., A.E. Christiansen, M. Costa, S. Parks, and E. Wieschaus. 1998. Hyperactivation of the folded gastrulation pathway induces specific cell shape changes. *Development.* 125:589–597.

Müller, H.A., and E. Wieschaus. 1996. Armadillo, bazooka, and stardust are critical for early stages in formation of the zonula adherens and maintenance of the polarized blastoderm epithelium in *Drosophila*. *J. Cell Biol.* 134:149–163. http://dx.doi.org/10.1083/jcb.134.1.149

Nikolaidou, K.K., and K. Barrett. 2004. A Rho GTPase signaling pathway is used reiteratively in epithelial folding and potentially selects the outcome of Rho activation. *Curr. Biol.* 14:1822–1826. http://dx.doi.org/10.1016/j.cub.2004.09.080

Oda, H., and S. Tsukita. 2001. Real-time imaging of cell-cell adherens junctions reveals that *Drosophila* mesoderm invagination begins with two phases of apical constriction of cells. *J. Cell Sci.* 114:493–501.

Rembold, M., L. Ciglar, J.O. Yáñez-Cuna, R.P. Zinzen, C. Girardot, A. Jain, M.A. Welte, A. Stark, M. Leptin, and E.E. Furlong. 2014. A conserved role for Snail as a potentiator of active transcription. *Genes Dev.* 28:167–181. http://dx.doi.org/10.1101/gad.230953.113

Sawyer, J.K., N.J. Harris, K.C. Slep, U. Gaul, and M. Peifer. 2009. The *Drosophila* afadin homologue Canoe regulates linkage of the actin cytoskeleton to adherens junctions during apical constriction. *J. Cell Biol.* 186:57–73. http://dx.doi.org/10.1083/jcb.200904001

Schäfer, G., M. Narasimha, E. Vogelsang, and M. Leptin. 2014. Cadherin switching during the formation and differentiation of the *Drosophila* mesoderm: Implications for epithelial-to-mesenchymal transitions. *J. Cell Sci.* 127:1511–1522. http://dx.doi.org/10.1242/jcs.139485

Shishido, E., S. Higashijima, Y. Emori, and K. Saigo. 1993. Two FGF-receptor homologues of *Drosophila*: One is expressed in mesodermal primordium in early embryos. *Development.* 117:751–761.

Smutny, M., H.L. Cox, J.M. Leerberg, E.M. Kovacs, M.A. Conti, C. Ferguson, N.A. Hamilton, R.G. Parton, R.S. Adelstein, and A.S. Yap. 2010. Myosin II isoforms identify distinct functional modules that support integrity of the epithelial zonula adherens. *Nat. Cell Biol.* 12:696–702. http://dx.doi.org/10.1038/ncb2072

Sweeton, D., S. Parks, M. Costa, and E. Wieschaus. 1991. Gastrulation in *Drosophila*: The formation of the ventral furrow and posterior midgut invaginations. *Development.* 112:775–789.

Truong Quang, B.A., M. Mani, O. Markova, T. Lecuit, and P.F. Lenne. 2013. Principles of E-cadherin supramolecular organization in vivo. *Curr. Biol.* 23:2197–2207. http://dx.doi.org/10.1016/j.cub.2013.09.015

Vincent, S., R. Wilson, C. Coelho, M. Affolter, and M. Leptin. 1998. The *Drosophila* protein Dof is specifically required for FGF signaling. *Mol. Cell.* 2:515–525. http://dx.doi.org/10.1016/S1097-2765(00)80151-3

Wang, Y.C., Z. Khan, M. Kaschube, and E.F. Wieschaus. 2012. Differential positioning of adherens junctions is associated with initiation of epithelial folding. *Nature.* 484:390–393. http://dx.doi.org/10.1038/nature10938

Wu, S.K., G.A. Gomez, M. Michael, S. Verma, H.L. Cox, J.G. Lefevre, R.G. Parton, N.A. Hamilton, Z. Neufeld, and A.S. Yap. 2014. Cortical F-actin stabilization generates apical-lateral patterns of junctional contractility that integrate cells into epithelia. *Nat. Cell Biol.* 16:167–178. http://dx.doi.org/10.1038/ncb2900

Xie, S., and A.C. Martin. 2015. Intracellular signalling and intercellular coupling coordinate heterogeneous contractile events to facilitate tissue folding. *Nat. Commun.* 6:7161.

Young, P.E., T.C. Pesacreta, and D.P. Kiehart. 1991. Dynamic changes in the distribution of cytoplasmic myosin during *Drosophila* embryogenesis. *Development.* 111:1–14.